

DOI: 10.1002/adma.200502721

Vapor-Phase Synthesis and Characterization of ϵ -FeSi Nanowires**

By Lian Ouyang, Elizabeth S. Thrall, Mandar M. Deshmukh, and Hongkun Park*

Over the past decade, one-dimensional inorganic nanostructures have emerged as promising materials for fundamental studies and possible technological applications.^[1–14] These structures exhibit physical and chemical properties distinct from their bulk counterparts as a result of radial confinement, while they retain the advantages of wirelike connectivity. In particular, silicon^[1,5] and silicide^[6] nanowires have received considerable attention owing to their potential ease of integration into conventional silicon-based electronics.

ϵ -FeSi is a narrow-bandgap semiconductor with a cubic structure (space group $P2_13$) that has been classified as a hybridization-bandgap semiconductor or Kondo insulator.^[15,16] It has attracted interest for over half a century, mainly because of its unusual magnetic behavior.^[17–21] Moreover, a recent study has identified doped iron monosilicides as potential alternatives to (GaMn)As and (GaMn)N in spintronics applications.^[22] Attempts to make FeSi thin films^[23–25] and nanorods^[26,27] embedded in silicon substrates have been reported in the past few years. To our knowledge, however, freestanding FeSi nanostructures have never been prepared, nor have magnetic or transport measurements been performed on embedded-rod or thin-film samples.

Here, we report the synthesis of single-crystalline FeSi nanowires and the characterization of their magnetic and electrical properties. The synthesis was performed using a chemical vapor deposition (CVD) method: silicon substrates were cleaned with 1 %-buffered HF and placed in a horizontal-tube furnace, between the center and the downstream end of the alumina tube. Anhydrous FeCl₃ powder (Aldrich, 99.99 %) was placed in an alumina boat upstream from the substrates. An inert atmosphere was maintained with a flow rate of 100 sccm N₂, and the temperature at the center of the furnace was set to 1100 °C. When the center of the furnace reached the set point, the iron source was hot enough (180–250 °C) to produce vapor-phase FeCl₃ or Fe₂Cl₆ without thermal decomposition. The precursor vapors were carried by the N₂ flow to the center of the furnace where they reacted with

silicon from the substrates. The reaction was held under these conditions for 1–2 h, and then the furnace was allowed to cool to room temperature. When the silicon substrates were taken out for examination, they were covered by a ‘fluffy’ black powder composed of aggregates of FeSi nanowires.

The morphology of the reaction product was examined using scanning electron microscopy (SEM) and transmission electron microscopy (TEM). Figure 1a shows representative SEM images, illustrating that the reaction produces two kinds of wires: single-stem wires and branched^[8,9] wires with triangular ‘thorns’ on their stems. Both SEM and TEM images reveal that the nanowire diameters range from 5 to about 100 nm and the lengths vary from a few hundred nanometers to tens of micrometers. The stoichiometry of the nanowire samples was assessed by energy-dispersive X-ray (EDX) spectrometry on individual wires using a high-resolution TEM (HRTEM) operating in scanning mode. In all the nanowires analyzed, Fe and Si were present in the correct 1:1 ratio (from 49 to 50.5 at % Si)^[28] within instrumental accuracy (see Supporting Information).

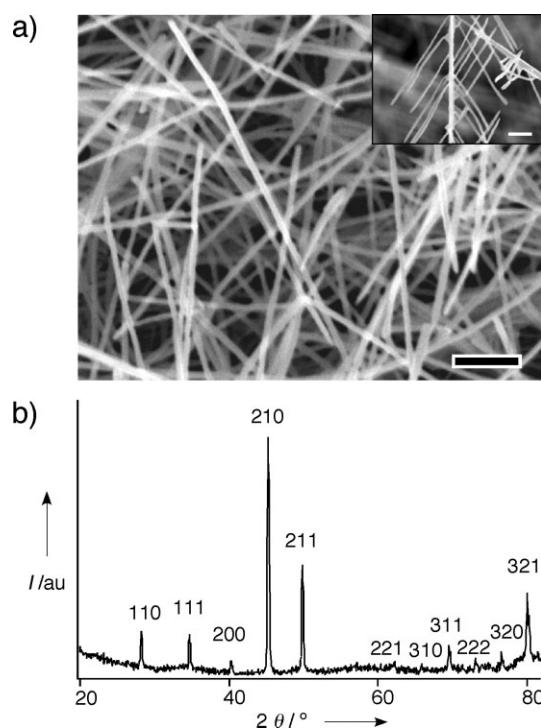


Figure 1. a) SEM image of ϵ -FeSi nanowires as grown on a silicon substrate. Inset: SEM image of a nanowire with both branches and triangular thorns. Both scale bars represent 500 nm. b) Powder XRD pattern of as-grown FeSi nanowires.

[*] Prof. H. Park, L. Ouyang, E. S. Thrall, Dr. M. M. Deshmukh
Department of Chemistry and Chemical Biology
Harvard University
Cambridge, MA 02138 (USA)
E-mail: HPark@chemistry.harvard.edu

[**] This work was supported by the National Science Foundation and the Packard Foundation. We thank Dr. J. Wu, Q. Gu for helpful discussions, and Dr. D. Bell, Y. Lu for technical assistance. Supporting Information is available online from Wiley InterScience or from the author.

Analysis of the powder X-ray diffraction (XRD) data shown in Figure 1b confirms that the nanowires are composed of crystalline FeSi with a cubic B20 structure. The unit-cell parameter for FeSi nanowires was determined to be 4.4880 Å, identical to that of the bulk cubic material (Joint Committee on Powder Diffraction Standards file 38-1397). Figure 2a shows a TEM image and a selected-area electron diffraction (SAED) pattern obtained from a representative FeSi nano-

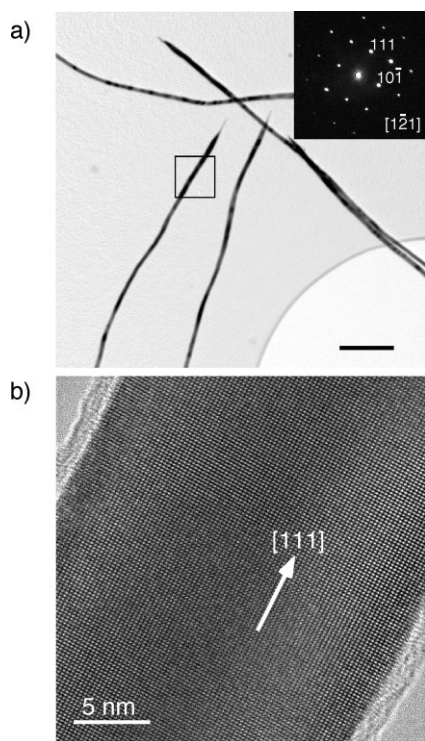
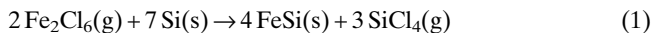
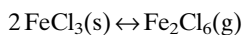


Figure 2. a) TEM image of a group of FeSi nanowires. Inset: SAED pattern from the area marked by the square. The SAED pattern is indexed for cubic FeSi nanowire down the $[1\bar{2}1]$ zone axis. The scale bar is 500 nm. b) HRTEM image of the same nanowire with growth direction parallel to the $[111]$ direction.

wire. The SAED pattern is indexed to a cubic ϵ -FeSi structure and demonstrates that the nanowire growth is along the $[111]$ direction. Notably, the diffraction pattern did not change as the electron beam (e-beam) was moved along the nanowire, indicating that the whole nanowire is a single crystal. Figure 2b shows a HRTEM image of a nanowire with clear lattice fringes, again confirming the material's high crystallinity. Further, the TEM and SAED data indicate that even branched nanowires, including the stem, branches, and thorns, are also single crystals (see Supporting Information). Because growth along any $[111]$ direction is equally favorable in a cubic structure, nanowires can branch out at an angle of 70.5° or 109.5° (the dihedral angles of two subsets of $[111]$ planes) while maintaining the integrity of the lattice, resulting in a single-crystalline branched wire.

The reaction that produces FeSi nanowires may involve multiple pathways because FeCl₃ evaporation produces many vapor species.^[29] Two plausible reaction paths are given by:



or



Several experimental observations suggest that FeSi nanowires are produced by a vapor–solid mechanism under a relatively low supersaturation ratio.^[3,12–14,30,31] First, the absence of catalyst particles at the ends of FeSi nanowires indicates that metal-catalyzed vapor–liquid–solid growth is unlikely. Second, the vapor pressure of the iron precursor was found to be critically important in nanowire growth: when the alumina boat containing FeCl₃ was positioned closer to the hot zone of the furnace only large chunks of FeSi were obtained, whereas in the opposite case no FeSi was produced at all. Higher temperatures at the alumina boat result in higher vapor pressures of Fe precursors and FeSi product in the reaction area, driving the supersaturation ratio above a critical point. Within the framework of the vapor–solid mechanism, this large supersaturation ratio favors bulk-crystal growth over nanowire growth,^[3,12,13,30,31] consistent with our experimental observations. Third, previous studies^[8] have shown that high supersaturation ratios can lead to nanowires with branched morphologies, again consistent with our experimental findings.

The magnetic properties of ϵ -FeSi nanowires were studied by measuring the sample magnetization as a function of temperature and applied magnetic field using a superconducting quantum-interference-device (SQUID) magnetometer. Figure 3a shows a plot of magnetization, M , versus temperature, T , for a nanowire ensemble. These curves were obtained by cooling the sample to $T=5$ K in the presence (field-cooled: FC) or absence (zero-field-cooled: ZFC) of a magnetic field, then recording M under an applied magnetic field of 50 kOe as the sample was warmed to 300 K. In both the FC and ZFC cases, the ensemble magnetization decreases as T increases to ca. 90 K and then rises again at higher T . This behavior compares well with published $\chi(T)$ data from both polycrystalline and single-crystalline bulk FeSi.^[17–20] Figure 3b shows plots of M versus applied magnetic field, H , at $T=5$ K and 300 K obtained from the same nanowire ensemble. The sample magnetizations at both temperatures are characterized by a small ‘ferromagnetic’ contribution riding on a dominant paramagnetic contribution (a linear increase in M as a function of magnetic field below $H=50$ kOe ($1\text{Oe}=1000/4\pi\text{A m}^{-1}$). This magnetic behavior is also consistent with that of single-crystalline bulk FeSi.^[21,32]

The electrical conductivity of individual FeSi nanowires was measured as a function of T by contacting them in a four-

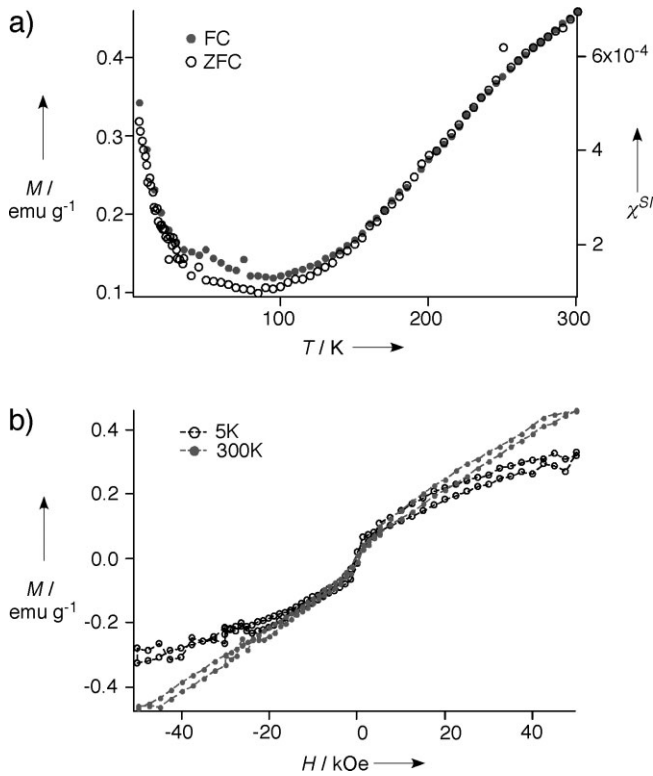


Figure 3. a) Plot of M versus T obtained from an FeSi nanowire ensemble. The filled and empty circles represent the FC and ZFC data, respectively. b) Plot of M as a function of H obtained from the same nanowire ensemble at 5 and 300 K.

probe geometry using e-beam lithography and thermally evaporated Cr–Au electrodes (Fig. 4, inset). Two different types of transport were observed in these samples. The first type, exhibited by single-stem nanowires without branches, is shown in Figure 4a. Here, the nanowire resistivity, ρ , falls over an order of magnitude when T is raised from 2 to 20 K. Following a plateau between 20 and 50 K, the resistivity drops steeply again, approaching a saturation value of ca. $2 \times 10^3 \mu\Omega\text{cm}$ at room temperature. This thermally activated behavior is similar to that observed in bulk FeSi:^[19,20] the drop in ρ below 20 K is attributed to the excitation of states within the bandgap, while the drop above 50 K reflects the increase in charge-carrier concentration, n_c , due to carrier excitation over the bandgap. Making the assumption that $n_c \propto 1/\rho$, the gap energy, E_g , can be extracted from the slope of $\ln(1/\rho)$ versus $1/k_B T$ using the thermal activation equation:^[33] $\ln(n_c) \propto \ln(1/\rho) \propto -E_g/(2k_B T)$. From a fit to the data in Figure 4a (see Supporting Information) between 93 and 193 K, E_g is found to be 50 meV, at the lower end of the range of E_g values reported for bulk FeSi.^[19,20]

The second type of transport behavior, exhibited primarily by nanowires with branches or thorns, is shown in Figure 4b. Here the resistivity rises between 5 and 50 K, followed by a fall to ca. $400 \mu\Omega\text{cm}$ at room temperature. The rise in ρ below 50 K is typical of a metal, while the fall at higher T is consis-

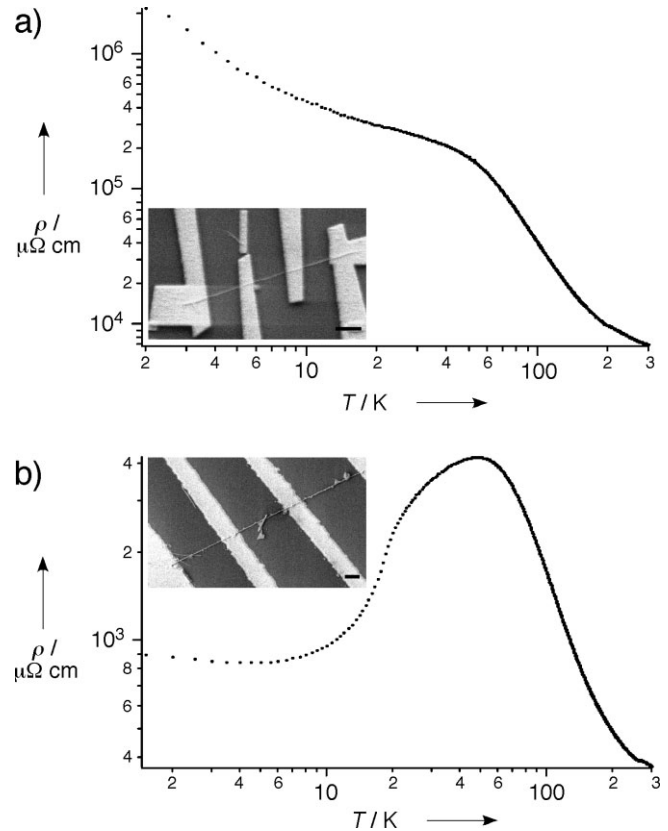


Figure 4. a) A plot of ρ as a function of T obtained from a representative single-stem nanowire. Here the nanowire diameter is 40 nm and the length between electrodes is 1.4 μm . Inset: SEM image of the nanowire device. b) A plot of ρ as a function of T obtained from a representative branched nanowire. The nanowire diameter is 45 nm and the length between electrodes is 3.8 μm . Inset: SEM image of the nanowire device. In (a) and (b) the scale bar in the inset is 1 μm .

tent with the thermal-activation behavior discussed above, with a bandgap of $E_g \approx 44$ meV (see Supporting Information). This crossover between metallic and semiconducting behavior is consistent with a heavily doped narrow-bandgap model, and suggests that branch-induced charge-carrier introduction may play a substantial role for branched FeSi nanowires. In this scenario, the Fermi energy lies within a conduction or a valence band in branched FeSi nanowires, and the transport is determined by a competition between the carrier scattering and the thermal excitation of carriers over the bandgap. At low T , where $\partial\rho/\partial T$ is positive, thermal energy is insufficient to change the charge-carrier concentration appreciably, and the increase in carrier scattering with T dominates. Above 50 K, excitation of carriers over the bandgap becomes significant, thereby lowering ρ . The fact that branched nanowires show metallic behavior at low temperatures suggests that the junctions between the stem and branches may act as a source of charge carriers, either by deviation from the ideal stoichiometry or by the introduction of lattice defects.

In conclusion, we have successfully synthesized freestanding single-crystalline nanowires of FeSi. The magnetic and electric

cal properties of the nanowires compare well with those of bulk materials, with some sample-specific variation. The synthesis of iron silicide nanowires reported here may provide a new synthetic route for nanoscale transition-metal silicides and may provide a platform for nanoscale spintronic applications.^[22]

Experimental

The morphology of the FeSi nanowires was analyzed with a LEO 982 field-emission scanning electron microscope and a JEOL 2010 transmission electron microscope with scanning TEM imaging and EDS X-ray-mapping capabilities. Powder XRD was performed at a scan rate of $0.10^\circ \text{ min}^{-1}$ using a Scintag XDS2000 X-ray diffractometer with a Cu K α radiation source. Ensemble nanowire magnetization was measured with a Quantum Design Magnetic Property Measuring System. For electrical-transport measurements, nanowires were deposited on a Si-SiO₂ wafer and located optically with respect to a coordinate grid. Electrodes were defined by e-beam lithography and thermally evaporated gold, with a thin (5–10 nm) primer layer of chromium. Electrical measurements were performed in an Oxford Instruments cryostat.

Received: December 21, 2005

Final version: March 8, 2006

Published online: April 26, 2006

- [1] J. Hu, T. W. Odom, C. M. Lieber, *Acc. Chem. Res.* **1999**, *32*, 435.
- [2] X. Peng, L. Manna, W. Yang, J. Wickham, E. Sher, A. Kadavanich, A. P. Alivisatos, *Nature* **2000**, *404*, 59.
- [3] Y. Xia, P. Yang, Y. Sun, Y. Wu, B. Mayers, B. Gates, Y. Yin, F. Kim, H. Yan, *Adv. Mater.* **2003**, *15*, 353.
- [4] M. Law, J. Goldberger, P. Yang, *Annu. Rev. Mater. Res.* **2004**, *34*, 83.
- [5] A. M. Morales, C. M. Lieber, *Science* **1998**, *279*, 208.
- [6] Y. Wu, J. Xiang, C. Yang, W. Lu, C. M. Lieber, *Nature* **2004**, *430*, 61.
- [7] A. I. Persson, M. W. Larsson, S. Stenstrom, B. J. Ohlsson, L. Samuelson, L. R. Wallenberg, *Nat. Mater.* **2004**, *3*, 677.
- [8] Z. A. Peng, X. Peng, *J. Am. Chem. Soc.* **2002**, *124*, 3343.
- [9] K. A. Dick, K. Deppert, M. W. Larsson, T. Martensson, W. Seifert, L. R. Wallenberg, L. Samuelson, *Nat. Mater.* **2004**, *3*, 380.
- [10] J. J. Urban, W. S. Yun, Q. Gu, H. Park, *J. Am. Chem. Soc.* **2002**, *124*, 1186.
- [11] J. J. Urban, E. S. Jonathan, L. Ouyang, W. S. Yun, H. Park, *Adv. Mater.* **2003**, *15*, 423.
- [12] B. S. Guiton, Q. Gu, A. L. Prieto, M. S. Gudiksen, H. Park, *J. Am. Chem. Soc.* **2004**, *127*, 498.
- [13] Z. R. Dai, Z. W. Pan, Z. L. Wang, *Adv. Funct. Mater.* **2003**, *13*, 9.
- [14] Z. W. Pan, Z. R. Dai, Z. L. Wang, *Science* **2001**, *291*, 1947.
- [15] G. Aeppli, Z. Fisk, *Comments Condens. Matter Phys.* **1992**, *16*, 155.
- [16] Z. Fisk, J. L. Sarrao, P. N. Cooper, G. S. Boebinger, A. Passner, P. C. Canfield, *Phys. B* **1996**, *223–224*, 409.
- [17] G. K. Wertheim, V. Jaccarino, J. H. Wernick, J. A. Seitchik, H. J. Williams, R. C. Sherwood, *Phys. Lett.* **1965**, *18*, 89.
- [18] V. Jaccarino, G. K. Wertheim, J. H. Wernick, L. R. Walker, S. Araj, *Phys. Rev.* **1967**, *160*, 476482.
- [19] Z. Schlesinger, Z. Fisk, H.-T. Zhang, M. B. Maple, J. F. DiTusa, G. Aeppli, *Phys. Rev. Lett.* **1993**, *71*, 1748.
- [20] S. Paschen, E. Felder, M. A. Chernikov, L. Degiorgi, H. Schwer, H. R. Ott, D. P. Young, J. L. Sarrao, Z. Fisk, *Phys. Rev. B* **1997**, *56*, 12916.
- [21] N. E. Sluchanko, V. V. Glushkov, S. V. Demishev, A. A. Menovsky, L. Weckhuysen, V. V. Moshchalkov, *Phys. Rev. B* **2002**, *65*, 064404.
- [22] N. Manyala, Y. Sidis, J. F. DiTusa, G. Aeppli, D. P. Young, Z. Fisk, *Nat. Mater.* **2004**, *3*, 255.
- [23] W. Huang, C. E. Zybilla, L. Luo, W. Hieringer, H. H. Huang, *Organometallics* **1998**, *17*, 5828.
- [24] H. von Kanel, K. A. Mader, E. Muller, N. Onda, H. Siringhaus, *Phys. Rev. B* **1992**, *45*, 13807.
- [25] U. Starke, W. Weiss, M. Kutschera, R. Bandorf, K. Heinz, *J. Appl. Phys.* **2002**, *91*, 6154.
- [26] M. Tanaka, F. Chu, M. Shimojo, M. Takeguchi, K. Mitsuishi, K. Furuya, *Appl. Phys. Lett.* **2005**, *86*, 183104.
- [27] M. Tanaka, M. Han, M. Takeguchi, K. Furuya, *Philos. Mag.* **2004**, *84*, 2699.
- [28] M. Hansan, K. Anderko, *Constitution of Binary Alloys*, 2nd ed., McGraw-Hill, New York **1958**.
- [29] L. E. Wilson, N. W. Gregory, *J. Phys. Chem.* **1958**, *62*, 433.
- [30] Y. Yin, G. Zhang, Y. Xia, *Adv. Funct. Mater.* **2002**, *12*, 293.
- [31] G. W. Sears, *Acta Metall.* **1955**, *3*, 361.
- [32] N. E. Sluchanko, V. V. Glushkov, S. V. Demishev, M. V. Kondrin, V. Y. Ivanov, K. M. Petukhov, A. A. Samarin, A. A. Menovsky, V. V. Moshchalkov, *JETP Lett.* **2001**, *92*, 312.
- [33] B. G. Streetman, S. Banerjee, *Solid State Electronic Devices*, 5th ed., Prentice-Hall, Upper Saddle River **2000**.